Research Square

Preprints are preliminary reports that have not undergone peer review.
They should not be considered conclusive, used to inform clinical practice,
or referenced by the media as validated information.

Role of Cdk5 in Mitochondrial Dysfunction: Phosphorylation of KANSL1 and Impairment of PINK1-Mediated Mitophagy

Binukumar B.K

binukumar@igib.res.in

CSIR Institute of Genomics and Integrative Biology,

Sangita Paul

CSIR Institute of Genomics and Integrative Biology, New Delhi, India. https://orcid.org/0000-0002-2419-2882

Juhi Bhardwaj

CSIR Institute of Genomics and Integrative Biology

Praveen Singh

CSIR- Institute of Genomics and Integrative Biology

Article

Keywords:

Posted Date: November 9th, 2026

DOI: https://doi.org/10.21203/rs.3.rs-10967273/v1

License: This work is licensed under a Creative Commons Attribution 4.0 International License.
Read Full License

Additional Declarations:

Table 3.2 is not available with this version

Tables are available in the Supplementary Files section.

Figures are available in the Supplementary Files section.

Role of Cdk5 in Mitochondrial Dysfunction: Phosphorylation of KANSL1 and Impairment of PINK1-Mediated Mitophagy

Sangita Paul[1,2], Juhi Bhardwaj[1,2], Praveen Singh[1,2], Binukumar BK[1,2*]

1. CSIR Institute of Genomics and Integrative Biology, New Delhi, India.

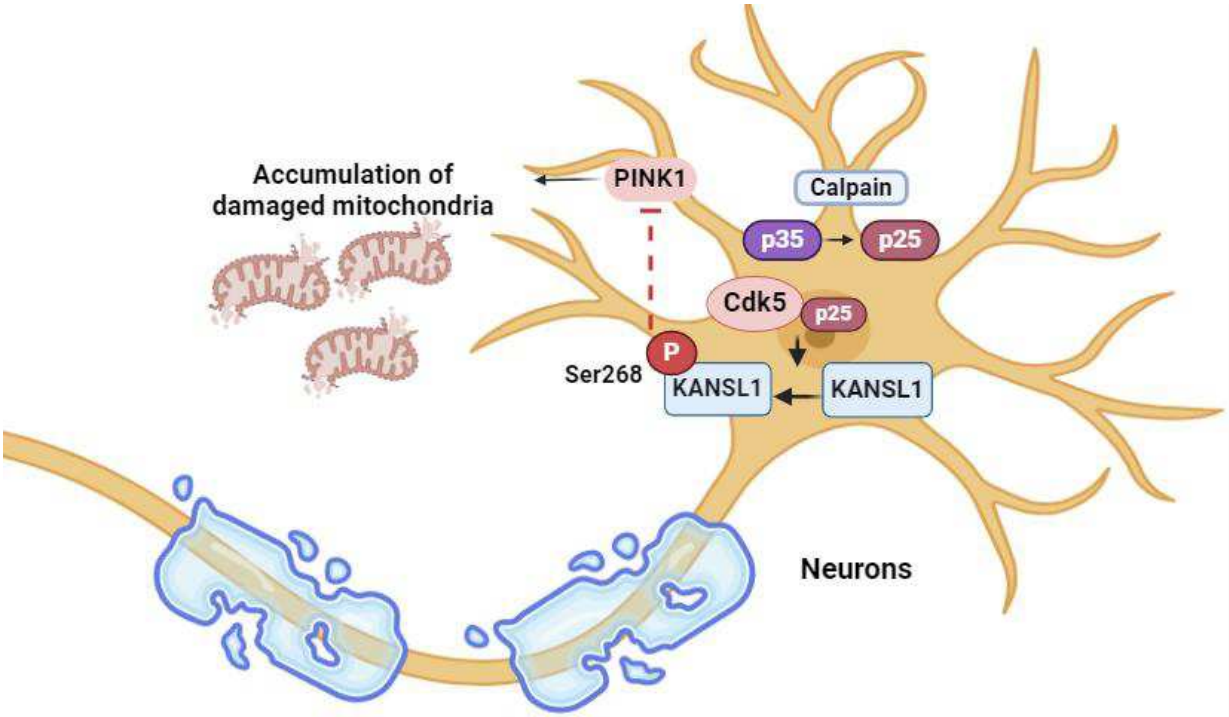
2. Academy of Scientific and Innovative Research (AcSIR), Ghaziabad- 201002, India.

[*]Correspondence to: Dr. Binukumar BK, Senior Principal Scientist, Genomics and Molecular Medicine, CSIR-Institute of Genomics and Integrative Biology (IGIB), Mathura Road, New Delhi 110025, India. binukumar@igib.res.in, binukumarbk@gmail.com

Abstract

Type 2 diabetes (T2D) is emerging as one of the most important risk factors for cognitive impairment and neurodegeneration, with mitochondrial dysfunction and defective mitophagy exacerbating disease progression. Despite the implication of aberrant cyclin-dependent kinase 5 (Cdk5) activation in T2D-neurodegeneration, the mechanisms linking Cdk5 hyperactivity to impaired mitochondrial quality control remain poorly defined. We therefore investigated whether Cdk5 regulates the epigenetic modulation of KAT8 Regulatory NSL Complex Subunit 1 (KANSL1), a newly discovered transcriptional regulator of PINK1-dependent mitophagy. Here in this study, we show that Cdk5 hyperactivation inhibits mitochondrial respiration, ATP generation, and mitophagy, leading to the accumulation of impaired mitochondria, while inhibition of Cdk5 by TFP5 rescues mitochondrial homeostasis in Cdk5-expressing neurons. The phosphoproteomic result revealed KANSL1 as a novel substrate of Cdk5, which specifically phosphorylates Ser268 of KANSL1. This study also demonstrates that Cdk5-mediated phosphorylation might decrease KANSL1 occupancy at the PINK1 promoter, attenuating its histone acetyltransferase activity to transcriptionally repress PINK1 expression, and may disrupt mitophagy. The upregulation of phospho-KANSL1 and downregulation of PINK1 were also validated in the brains of HFD-induced T2D mice. Our combined results reveal a previously unknown Cdk5–KANSL1–PINK1 signaling axis that connects the relationship of Cdk5 hyperactivation to mitochondrial quality control defects and positions

KANSL1 phosphorylation as an alluring novel therapeutic target for neurodegeneration associated with diabetes.



Keywords

Mitochondria, phosphorylation, Type 2 diabetes, Neurodegeneration, Cdk5, KANSL1

Bullet Points

- Cdk5 hyperactivation impairs mitochondrial respiration, ATP production, and mitophagy in neurons, promoting the accumulation of dysfunctional mitochondria.
- Cdk5 inhibition by TFP5 restores mitochondrial homeostasis, highlighting Cdk5 as a potential therapeutic target.
- KANSL1 is identified as a novel Cdk5 substrate, with Cdk5 specifically phosphorylating KANSL1 at Ser268.
- Cdk5-mediated KANSL1 phosphorylation reduces KANSL1 occupancy at the PINK1 promoter, suppressing PINK1 expression and disrupting PINK1-dependent mitophagy.

- The Cdk5–KANSL1–PINK1 signaling axis is dysregulated in T2D, suggesting KANSL1 phosphorylation as a potential therapeutic target for diabetes-associated neurodegeneration.

Introduction

Type 2 diabetes (T2D) is a chronic metabolic disease characterized by long-lasting severe hyperglycemia and insulin resistance, affecting multiple organs, including the central nervous system. A growing body of clinical and experimental evidence has shown that chronic metabolic stress, oxidative damage, neuroinflammation, and impaired neuronal survival in patients with T2D are associated with an increased risk of cognitive decline and neurodegenerative disorders, including Alzheimer's disease (AD) [1,2]. Despite these multifactorial mechanisms responsible for the progression of diabetes-associated neurodegeneration, mitochondrial dysfunction is emerging as one of the earliest and most critical pathological processes in synaptic failure and neuronal loss [3,4].

Cyclin-dependent kinase 5 (Cdk5) is a serine/threonine kinase that is enriched in neurons and exerts its essential roles in neuronal development, synaptic plasticity, cytoskeletal organization, and survival of neurons under physiological conditions (Dhavan and Tsai, 2001). Cdk5 is distinctive among cyclin-dependent kinases in that its activation depends on neuron-specific cofactors, p35 and p39, rather than on cyclins. Under pathological circumstances like oxidative stress, calcium dysregulation and metabolic insults characteristic of type 2 diabetes (T2D), p35 is proteolytically cleaved by calpain to the truncated fragment p25, permitting a sustained and ectopic activation of Cdk5 [5–8]. Cdk5 hyperactivation is believed to play a central role in the pathogenesis of numerous neurodegenerative diseases, such as AD, PD, ALS and diabetic cognitive impairment via induction of tau hyperphosphorylation (HP), neuroinflammation, oxidative stress, mitochondrial dysfunction and neuronal apoptosis [9–11]. In accordance with these observations, independent studies from our laboratory reported that the pharmacological inhibition of Cdk5 hyperactivity using the peptide inhibitor TFP5 reduces neuroinflammation, ameliorates mitochondrial functions, and improves cognitive performance in experimental models for T2D [12–15]. However, the molecular substrates through which dysregulated Cdk5 activity disrupts mitochondrial homeostasis in vivo remain largely unknown.

Mitochondrial quality control, in particular mitophagy (the selective autophagic removal of dysfunctional mitochondria), is critical for the maintenance of mitochondrial homeostasis [16]. The PINK1–Parkin pathway is the best characterized mechanism regulating mitophagy. Under physiological conditions, PINK1 is continuously imported into intact mitochondria, followed by fast degradation. In contrast, damaged mitochondria increase PINK1 stabilization on the outer mitochondrial membrane (OMM), thereby recruiting and activating Parkin to promote ubiquitin-dependent clearance of dysfunctional mitochondria via the autophagy–lysosome pathway [17,18]. Emerging evidence supports that defective PINK1-dependent mitophagy may underlie mitochondrial dysfunction and neuronal degeneration in neurodegenerative disorders and diabetes [19–21]. However, the upstream mechanisms regulating PINK1 transcription under diabetic conditions are largely unexplored.

Recent studies have shown that KANSL1 (KAT8 regulatory NSL complex subunit 1) encodes an important transcriptional regulator of PINK1. KANSL1 is a component of the NSL (Non-Specific Lethal) histone acetyltransferase complex that activates transcription by both acetylation of histone H4 and chromatin remodeling [22–24]. Genome-wide studies confirmed direct binding of the NSL complex to the PINK1 promoter, regulating its transcription and maintaining mitochondrial quality control and mitophagy [25]. Studies have even associated KANSL1 deficiency with neuronal homeostasis due to impaired mitochondrial function and neurodevelopmental disorders [23]. Although KANSL1 has recently emerged as a key regulator of mitochondrial quality control, it is unclear whether its expression in the face of mitochondrial stress during pathological stimulation is subject to post-translational modifications.

Notably, KANSL1 was found to contain a conserved Cdk5 consensus phosphorylation site (the peptide sequence KSP) centered on the residue Ser268, indicating that it may be a direct substrate of Cdk5 as determined from sequence analysis. Based on this information, we hypothesized that aberrant Cdk5 activation downregulates PINK1-dependent mitophagy through phosphorylation of KANSL1 to inhibit its transcriptional activity. Of course, we set out to challenge our hypothesis using mitochondrial bioenergetic analysis, phosphoproteomics, site-directed mutagenesis, chromatin immunoprecipitation, and histone acetyltransferase assays coupled with in vivo validation by utilizing a high-fat diet-induced T2D mouse model. We demonstrate KANSL1 as an

undiscovered substrate of Cdk5 and establish a novel Cdk5–KANSL1–PINK1 signalling axis connecting Cdk5 hyperactivation to impaired mitochondrial function and mitophagy in diabetic neurodegeneration.

Materials and Methods

Mitostress-Experiment with Seahorse XF24

Neuro2A (N2A) cells were utilized for the neuronal cell culture experiments and confirmed to be mycoplasma-negative. After seeding in XF24 microplates for 12 hours, N2A cells were transfected with Cdk5/p35 and Cdk5/p25 complexes. Twelve hours post-transfection, the cells were treated with the Cdk5 inhibitor TFP5. Following 24 hours of treatment, the cells underwent mitostress analysis using the XF-24 Seahorse instrument. Each well contained final concentrations of 2 μM oligomycin, 0.8 μM FCCP, and 2 μM each of antimycin and rotenone. The oxygen consumption rate (OCR) was normalized to protein content in each well, determined by the BCA assay. Results were analyzed using Wave Desktop software, with additional statistical analysis performed using GraphPad Prism.

Transfection

N2A cells were co-transfected with plasmids encoding Cdk5 and either p35 or p25 to generate the Cdk5/p35 and Cdk5/p25 complexes, respectively. The p35 and p25 constructs contained a Myc epitope tag to facilitate confirmation of transfection efficiency by immunoblotting. Cells were seeded 12 h prior to transfection, and a total of 2 μg plasmid DNA per well was transfected using 1 μg of Cdk5 plasmid together with 1 μg of either p35 or p25 plasmid. Twenty-four hours after transfection, cells were treated with TFP5, a selective inhibitor of Cdk5/p25 activity, while cells treated with the scrambled control peptide (SCP) served as the negative control. Cells were harvested after the indicated treatment period for subsequent biochemical and functional analyses.

Mitochondrial number counting per cell

Following cotransfection with Cdk5 complexes and treatment with the inhibitor TFP5, N2A cells underwent mitochondrial staining using MitoTracker Red (Catalog number: M7512) according to the product protocol. The stained cells were imaged with a confocal microscope to count the

mitochondria per cell using ImageJ Fiji software. Microscopy images were opened in the software, and individual cells were selected. The image was split into red, green, and blue channels, with the green channel highlighting mitochondria. The following filters were applied sequentially: sharpen, despeckle, background subtraction, local contrast enhancement, and 'tubeness' (sigma = 0.0210) to enhance filamentous structures. The image was then converted to binary after applying a Gaussian blur (sigma radius = 1.000). The processed image was used to analyze mitochondrial number and length [31].

Mitochondrial DNA (mtDNA) copy number analysis

Relative mitochondrial DNA (mtDNA) copy number was determined by quantitative real-time PCR (qPCR). Total DNA, containing both mitochondrial and nuclear genomic DNA, was extracted from N2A cells using the phenol–chloroform protocol [32,33]. DNA concentration and purity were assessed using a NanoDrop spectrophotometer, and equal amounts of DNA (50 ng) were used for each qPCR reaction. Quantitative PCR was performed using PowerUp™ SYBR™ Green Master Mix (Applied Biosystems, USA) on a QuantStudio™ 5 Real-Time PCR System (Applied Biosystems). Relative mtDNA content was determined by amplifying the mitochondrial NADH dehydrogenase subunit 1 (ND1) gene [32]and normalized to the single-copy nuclear β2-microglobulin (B2m) gene [34]. Relative mitochondrial DNA copy number was calculated as the mtDNA-to-nuclear DNA ratio using the 2^−ΔΔCt method and expressed as fold change relative to the control group.

Primer sequences:

Mouse ND1 (mtDNA)

FWD: 5’-CTAGCAGAAACAAACCGGGC-3’

REV: 5’-CCGGCTGCGTATTCTACGTT-3’

Mouse β2-microglobulin (B2m, nuclear DNA)

Forward: 5′-ATGGGAAGCCGAACATACTG-3′

Reverse: 5′-CAGTCTCAGTGGGGGTGAAT-3′

Assessment of Mitophagic Flux Using Bafilomycin A1

Bafilomycin A1 (BafA1) is a lysosomal V-ATPase inhibitor that inhibits the fusion of autophagosomes and lysosomes, as well as lysosomal acidification, which was used to evaluate mitophagic flux. In brief, N2A cells were transfected with different doses of Cdk5/p25 or Cdk5/p35

expression constructs and treated with TFP5 as indicated. N2A cells were seeded and cultured to achieve 70% confluency before transfection. The cells were transiently co-transfected with plasmid constructs encoding either CDK5/p25 with/without 500nM TFP5, or CDK5/p35, utilizing Lipofectamine 3000 in accordance with the manufacturer's optimized protocol. Twenty-four hours post-transfection, the cells were treated with 20 nM Bafilomycin A1 (BafA1) for 4 hours. Control groups received an equivalent volume of DMSO (vehicle).

Western blot

Cell and tissue lysates were prepared using RIPA buffer containing 1X protease and 1X phosphatase inhibitor cocktails. Each well of a 10% SDS gel was loaded with 30 µg of protein. Proteins were transferred onto nitrocellulose membranes, and stripping was performed using a Thermo stripping buffer (Catalog number: 46430). The antibodies used are listed in Table 1.

Site-Directed Mutagenesis

The plasmid for KANSL1 was purchased from Add Gene (Catalog no. 29758). Site-directed mutagenesis (SDM) was performed using an Agilent SDM kit. The reaction mixture was set up as suggested by the Agilent protocol. The PCR cycle is mentioned in Table 3.2.

The primer sequences used for generating the SDM are:

Primer Sequence (5'; to 3')

Serine to Alanine

5'-TGAAAAGAATGGAAGACAGGGGAGCCTTTTTACCCTCCAATTTGACACC-3'5'-GGTGTCAAATTGGAGGGTAAAAAGGCTCCCCT**GTC**TTCCATTCTTTTCA-3';

Serine to Glutamate

5'-TGAAAAGAATGGAAGACAGGGGCTCCTTTTTACCCTCCAATTTGACACC-3'

5'-GGTGTCAAATTGGAGGGTAAAAAG**GAG**CCCCTGTCTTCCATTCTTTTCA-3'

Immunoprecipitation

Immunoprecipitation was performed using protein A/G agarose beads. The protocol was followed as described in our previous publication[10]. The beads were incubated with constant agitation for 4-6 hours with 2 µg of the antibody of interest (KANSL1 and Cdk5). Samples were dissolved in 200 µl lysis buffer (20 mM Tris-HCl HCl pH 8, 137 mM NaCl, 1% NP-40, 2 mM EDTA). After incubation,

beads were collected by centrifugation at 13,000 rpm for 20 minutes at 4°C and washed three times with lysis buffer. The antibody-conjugated beads were mixed with 100 µg lysate and incubated overnight at 4°C. The beads were centrifuged again, washed three times with lysis buffer, and eluted using 50 µl of urea buffer (8 M urea, 20 mM Tris, pH 7.5, 100 mM NaCl) with constant agitation and centrifugation at 13,000 rpm for 20 minutes at 4°C.

Chromatin-immunoprecipitation (ChIP)-qPCR assay

ChIP was performed with minor modifications to the protocol described by Nelson et al. (2006)[35]. Briefly, N2A cells were cross-linked with 1% formaldehyde for 10 min at 37°C, and the reaction was quenched with 125 mM glycine for 5 min. Cells were washed with ice-cold PBS containing a protease inhibitor cocktail and lysed in SDS lysis buffer. Chromatin was sheared by sonication using a Bioruptor™ UCD-200 (Diagenode) to obtain DNA fragments averaging 200–500 bp, and the fragment size was verified by agarose gel electrophoresis. Equal amounts of chromatin were incubated overnight at 4°C with an anti-KANSL1 antibody (2ug) on a rotating platform, followed by capture with pre-blocked protein A/G magnetic beads for 4 h. The immunoprecipitated complexes were sequentially washed with low-salt, high-salt, LiCl, and TE buffers to minimize non-specific binding. Protein–DNA cross-links were reversed following proteinase K digestion, and DNA was purified by phenol:chloroform:isoamyl alcohol extraction followed by isopropanol precipitation. Purified DNA was resuspended in nuclease-free water and subjected to qPCR using primers specific for the mouse PINK1 promoter. ChIP enrichment was calculated relative to the input DNA and expressed as a percentage of input [36].

PINK1 promoter primer sequences:

Seq1:

Forward Primer: CCGGCTTTGTTGATTGGCAG

Reverse Primer: CCTTATTGGCGAAACGCACT

Seq 2:

Forward Primer: GGACCAAGAAGCAGGGAACG

Reverse Primer: AGCCCGTTAGACTAGCGACA

In vitro transcription and translation

In vitro transcription and translation of FLAG-tagged KANSL1 wild type and mutants were performed using the PURExpress® In Vitro Protein Synthesis Kit (New England Biolabs, Ipswich, MA, USA) according to the manufacturer's instructions. Briefly, a T7 promoter-driven FLAG-KANSL1 plasmid was used as the template for coupled transcription and translation, and the reaction was incubated at 37°C for 2 h. Protein synthesis was confirmed by immunoblotting using an anti-FLAG antibody [37]. The synthesized FLAG-KANSL1 protein was subsequently used for in vitro kinase assays with commercially available recombinant Cdk5/p25 and Cdk5/p35 complexes (Sigma-Aldrich, St. Louis, MO, USA), followed by LC–MS/MS phosphoproteomic analysis to identify Cdk5-dependent phosphorylation sites.

In vitro Cdk5 kinase assay

Cdk5/p25 and Cdk5/p35 complexes were assayed for kinase activity using the ADP-Glo™ Kinase Assay (Promega, Madison, Wisconsin, USA) according to the manufacturer's instructions. In vitro-translated FLAG-KANSL1 protein was treated with recombinant Cdk5/p25 or Cdk5/p35 (Sigma-Aldrich, St. Louis, MO, USA) in kinase reaction buffer containing ATP (10 μM) at 30°C for 60 min. Kinase buffer was used for sample preparation with a composition of 50 mM Tris-HCl (pH 7.5),10 mM $MgCl_2$,1 mM DTT**.** We furthermore included control reactions that lacked kinase or substrate to measure background activity. After the kinase reaction, ADP-Glo™ Reagent was added to stop the reaction and deplete the unconsumed ATP, followed by Kinase Detection Reagent to convert any leftover ADP produced during the kinase reaction back into ATP, which then generates a luminescent signal proportional to kinase activity. Luminescence detection was performed using a SpectraMax i3x Multi-Mode Microplate Reader (Molecular Devices, USA) [12,26].

Custom-made Phospho-specific antibody

The custom-made Anti-KANSL1(pSer) antibody was generated by the Biomatik Antibody Group. Phosphopeptide sequence: Cys-NLGGVKLEGKK(pS)PLSS; lot A230210-SF013507, Non-phosphopeptide: Cys-NLGGVKLEGKKSPLSS, lot: A230210-SF013508, host stain: Rabbit. The KANSL1_268-phospho-antigen Cys-NLGGVKLEGKK(pS)PLSS was injected to immunize the rabbit. After the separation, the serum was removed using a KANSL1 non-phosphopeptide affinity column. The flow-through was also passed through a phosphopeptide affinity column for affinity purification. The antibodies attached to the phosphopeptide column were eluted and then

characterized by indirect ELISA. For antibody characterization, phosphopeptides and nonphosphopeptides were coated with PBS, pH 7.4, at concentrations of 4 µg/ml and 100 µl/well, respectively. The secondary antibody used in the ELISA was an anti-rabbit IgG monoclonal antibody.

Immunocytochemistry

Immunocytochemistry was performed on N2A cells seeded on poly-D-lysine-coated coverslips. After 24 hours, the cells were fixed with chilled methanol for 5 minutes and washed with 1X PBS. The fixed cells were then incubated overnight with KANSL1 and Cdk5 antibodies, followed by secondary antibody incubation for 2 hours. The cells were stained with DAPI and mounted with antifade mounting media. Slides were sealed with nail polish before confocal imaging. Images were captured using a Nikon Eclipse Ti2 confocal microscope with a 60X oil immersion objective lens. Colocalization was calculated using ImageJ software with the JacoP plugin, which provides Pearson's colocalization coefficient for two channels of interest.

Histone acetyltransferase activity (HAT) assay

The histone acetyltransferase activity was measured using a commercially available HAT assay kit from Abcam (catalog no. ab65352). The experiment was performed using the protocol suggested by the kit, and the calculation was done accordingly.

HFD mice model generation

All animal experiments were approved by the Institutional Animal Ethics Committee (IAEC) of the CSIR–Institute of Genomics and Integrative Biology (CSIR-IGIB) and conducted in accordance with the relevant institutional guidelines for the care and use of laboratory animals. Male C57BL/6 mice (n = 6 per group) were used in this study. A high-fat diet (HFD) was administered for three months to establish a Type 2 diabetes (T2D) mouse model, following the experimental protocol described previously by Paul et al. (2024)[11]. Age-matched mice maintained on a standard chow diet served as controls

Real-time PCR

RNA was isolated from the brain tissues through the Trizol method, followed by chloroform layering and precipitation with isopropanol. The RNA quality was checked through agarose gel electrophoresis. The RNA was then converted to cDNA using the protocol suggested by the cDNA synthesis kit (RevertAid First Strand cDNA Synthesis Kit, catalog no.: K1621). The cDNA was then utilized to perform RT-PCR.

The primers used for the RT-PCR experiment is specific to the PINK-1 gene, and the loading control used was specific to the GAPDH gene. The sequence of the primers is as follows:

GAPDH Forward primer: TCCCCTTAGTTCGAGGGACT

GAPDH Reverse primer: ACATCACCCCCATCACTCAT

PINK-1 Forward primer: GTGGGACTCAGATGGCTGTC

PINK-1 Reverse primer: CCATTGCCACCACGCTCTAC

Phospho-proteomics using LC-MS

Phospho-proteomics is a process that typically begins with the lysis of cells or tissues in a buffer containing protease and phosphatase inhibitors to preserve phosphorylation states, followed by protein quantification using assays like BCA or Bradford. Proteins are then reduced, alkylated, and digested into peptides with trypsin. The resulting peptide mixture undergoes desalting using C18 solid-phase extraction. Phosphopeptides are enriched using immobilized metal affinity chromatography (IMAC) or titanium dioxide (TiO2) beads, which are then eluted with an acidic buffer. These enriched phosphopeptides are separated via liquid chromatography and analyzed by a high-resolution mass spectrometer using data-dependent acquisition (DDA) to identify phosphorylation sites. The raw data is processed with software like MaxQuant or Mascot, where phosphorylation is searched as a variable modification [38–40]. Quantified phosphopeptides are then analyzed using bioinformatics tools to identify affected pathways, with key phosphorylation sites validated by methods such as Western blotting using phospho-specific antibodies.

Statistical analysis

GraphPad Prism version 5.0 was used to perform all statistical analyses. Data are shown as mean ± standard error of the mean (SEM) from at least three independent biological replicates. Each figure legend includes the sample size (n) used for each experiment. The Kolmogorov–Smirnov test was

used to check the normality of data distribution before statistical testing. An unpaired two-tailed Student's t-test was performed on comparisons of two independent groups. Data for three groups or by group comparisons were analyzed with one-way analysis of variance (ANOVA), followed by Tukey's multiple comparisons post hoc test to determine pairwise differences between groups. The statistical test used for each dataset is specified in the individual figure legends where applicable. P value < 0.05 was used to determine statistical significance between the groups. The figures depict statistical significance represented as follows: $*P < 0.05$, $**P < 0.01$, $***P < 0.001$, non-significant differences are denoted "ns" where appropriate.

Results

Cdk5 hyperactivation promotes mitochondrial stress and accumulation in N2A cells

In order to elucidate the effects of Cdk5 hyperactivity on mitochondrial function and mitophagy, N2A cells were co-transfected with constructs that express Cdk5/p35 and a hyperactive complex of Cdk5/p25. After transfection, cells were treated with the Cdk5 selective inhibitory peptide TFP5 [14], and a negative control scrambled peptide (SCP) was added to further validate any effects mediated by TFP5.

Mitochondrial stress was studied using a Seahorse XF-24 analyser. Oxygen consumption rate (OCR). Basal respiration, maximal respiration, ATP-linked respiration, and spare respiratory capacity parameters were assessed. The results revealed that overexpression of Cdk5/p35, and particularly Cdk5/p25, profoundly inhibited all mitochondrial respiratory parameters (Figures 1A–B), suggesting that it exerts deleterious effects on mitochondria. Overall, the most critical finding was that TFP5 treatment effectively ameliorated mitochondrial stress, regardless of the amplitude of Cdk5 activity. Hence, inhibition of Cdk5 activity rescues mitochondrial bioenergetic deficits induced by hyperactivation of this kinase.

Mitochondrial integrity was evaluated in Cdk5/p25-transfected cells with or without TFP5 treatment by staining the mitochondria with MitoTracker Red. Cdk5/p25 overexpression led to a major build-up of mitochondria, while TFP5 strongly hampered this accumulation (Figures 1C and D),

suggesting that Cdk5 hyperactivation allows dysfunctional mitochondria to persist because they are unable to be cleared out.

Cdk5 hyperactivity leads to impaired mitophagy through PINK1 downregulation

Since the previous experiments indicated mitochondrial dysfunction and an increase in the number of mitochondria per cell after Cdk5 hyperactivation, we next investigated whether mitophagy was dysregulated by Cdk5 hyperactivity. A: Representative Western blot of mitophagy proteins (PINK1, PARKIN, LC3-I, LC3-II, and p62) expression in the Cdk5/p25 overexpressed group with or without TFP5 treatment. In N2A cells, Cdk5 activity increased dramatically, leading to a significant down-regulation of PINK1 and LC3-II expression with upregulation of p62 by blocking mitophagy, which resulted in impaired clearance of damaged mitochondria (Figure 2A-E).

Mitophagy flux was then measured in basal conditions and after exposing cells to the lysosomal inhibitor Bafilomycin A1 (BafA1), which blocks autophagosome–lysosome fusion and allows quantification of autophagic flux, to determine if mitochondrial accumulation occurred due to defective mitophagy. We thus conducted parallel analyses in the presence and absence of BafA1 to differentiate impaired degradation of mitochondria from alterations in mitochondrial biogenesis. In line with the decrease in PINK1 expression, Cdk5/p25-overexpressing cells displayed defective mitophagy as indicated by decreased mitochondrial clearance at basal conditions and a reduced response to BafA1 treatment compared to control cells. By contrast, TFP5 treatment re-established mitophagy flux, reflecting that Cdk5 inhibition rescues PINK1-dependent mitochondrial quality control. These results suggest that collectively Cdk5 hyperactivation promotes mitochondrial dysfunction via a dual mechanism of both inhibition of mitochondrial respiration and suppression of PINK1-mediated mitophagy, leading to accumulation of damaged mitochondria.

Cdk5 phosphorylates KANSL1 at Serine-268

Recent studies show that KANSL1, a key component of the Non-Specific Lethal (NSL) complex, is essential for PINK1 transcription and for mitophagy-mediated regulation [22]. Notably, KANSL1 has a putative Cdk5 consensus phosphorylation site (KSP) at Ser268 and may be a potential direct

substrate of Cdk5. This was addressed by overexpressing FLAG-tagged KANSL1 in N2A cells, immunoprecipitations, and an in vitro kinase assay in the presence or absence of the Cdk5/p25 complex from mouse brain cell lysate then LC–MS/MS-based phosphoproteomic analysis (Figure 3A). In a mass spectrometric analysis of immunoprecipitated KANSL1, the phosphorylated peptide NLGGVKLEGKK(pS)PLSS (containing Ser268) was identified as the site of Cdk5 phosphorylation through its identification in both panels (Figure 3B–C). Subsequently, a quantitative phosphoproteomic analysis confirmed that Cdk5/p25 treatment led to an increase of 4.1-fold in the phosphorylation of Ser268 ($p = 0.003$; Figure 3D), thus showing KANSL1 as a new substrate for Cdk5. These results uncover Ser268, a novel Cdk5 phosphorylation site on KANSL1 and indicate that dysregulated Cdk5 activity may control KANSL1 function through posttranslational modification, which thus provides potential mechanistic understanding of how aberrant Cdk5 activation disturbs PINK1-dependent mitophagy.

In order to confirm that Ser268 is the functional Cdk5 phosphorylation site, phospho-deficient (S>A) and phospho-mimetic (S>E) KANSL1 mutants were generated by site-directed mutagenesis and verified by Sanger sequencing (Figures 4A–B). Using in vitro kinase assays, we found that both Cdk5/p35 and the hyperactive Cdk5/p25 complex phosphorylated wild-type KANSL1 robustly, but not S>A (Figure 4C–E), confirming Ser268 as the main target residue for phosphorylation by Cdk5. Immunoblotting with a phospho-Ser268-specific antibody revealed robust phosphorylation of wild-type KANSL1, but only little or undetectable signal for the S>A mutant, even though protein expression levels were similar for all constructs (Figure 4F). In addition, the selective Cdk5 inhibitor TFP5 significantly inhibited KANSL1 phosphorylation mediated by Cdk5, while the scrambled control peptide did not (Figure 4G). Together, these results confirm that KANSL1 acts as a substrate of Cdk5 and its phophorylation site is Ser268.

Cdk5 Associates with KANSL1 and Influences Its Chromatin Occupancy at the PINK1 Promoter

To establish a direct association of KANSL1 with Cdk5, reciprocal co-immunoprecipitation assays were carried out in N2A cells overexpressing KANSL1 along with the Cdk5/p35 and Cdk5/p25 complex (Figure 5B). Immunoprecipitation for KANSL1 effectively pulled down Cdk5 (Figure 5B). This interaction was also seen in Cdk5/p35- and Cdk5/p25-transfected cells, again suggesting that

KANSL1 interacts with Cdk5 regardless of its activator. To further confirm this interaction in situ, we did an immunocytochemical analysis in the N2A cells. Positive co-localization of endogenous Cdk5 and KANSL1 was conclusively shown by confocal microscopy, as evidenced by a high degree of overlap of the green (Cdk5) and red (KANSL1) fluorescence signals in their merged images (Figure 5C) with a Pearson's coefficient of 0.66. Combined, these biochemical and imaging approaches demonstrate that KANSL1 is a Cdk5 interactor in neural cells.

Since KANSL1 acts as a transcriptional regulator that localizes to chromatin, we also examined whether Cdk5 activation influences its binding to the PINK1 promoter. Using chromatin immunoprecipitation (ChIP)-qPCR with an anti-KANSL1 antibody, we observed a high enrichment of the PINK1 promoter in KANSL1-overexpressing cells compared to non-transfected controls, providing direct evidence of KANSL1 occupancy at the PINK1 promoter (Figure 5D,E). Notably, Cdk5/p35 and Cdk5/p25 co-expression markedly diminished KANSL1 enrichment at the PINK1 promoter (Figure 5E). Together, these results reveal Cdk5 hyperactivation compromised recruitment of KANSL1 to the PINK1 promoter as a mechanistic explanation for decreased transcription of PINK1 in response to dysregulated Cdk5

Cdk5 hyperactivity inhibits KANSL1-dependent PINK1 transcription, contributing to mitophagy impairment

Now that we have demonstrated Cdk5 phosphorylates KANSL1 at Ser268 and negatively regulates its recruitment to the PINK1 promoter, we next investigated if this phosphorylation impacts on KANSL1-mediated transcriptional regulation of PINK1. N2A cells were transfected with KANSL1 alone, along with a combination of Cdk5/p35 and hyperactive Cdk5/p25 complex, followed by evaluation of p-KANSL1 and PINK1 expression (Figure 6A). When co-expressed with KANSL1, both Cdk5/p35 and Cdk5/p25 (more prominently) enhanced the phosphorylation of KANSL1 along with a gradual decrease in PINK1 protein levels compared with KANSL1 alone, as shown by western blot analysis (Figure 6B–C). In agreement with these results, quantitative PCR analysis showed a substantial reduction in PINK1 mRNA levels in cells expressing the Cdk5/p25 complex (Figure 6D) and thus together suggested that KANSL1 phosphorylation by Cdk5 serves to suppress the expression of PINK1 at the transcriptional level. KANSL1 acts as part of the NSL HAT (histone

acetyltransferase) complex, so we next tested whether it has in vitro HAT activity. Importantly, HAT activity of NSL complex was inhibited by overexpression of KANSL1 with Cdk5/p35 and especially Cdk5/p25, whereas the phospho-deficient KASNL1 S > A mutant retained this activity even when co-expressed with Cdk5/p25. In contrast, the phospho-mimetic KANSL1 S>E mutant showed a constitutive decrease in NSL complex HAT activity that was not further impacted by Cdk5/p25 (Figure 6F). The results collectively show that Cdk5 phosphorylation on KANSL1 at Ser268 inhibits histone acetyltransferase activity of the NSL complex to repress PINK1 transcription, and also for the first time link Cdk5 hyperactivation to impaired mitophagy in a mechanistic manner.

In vivo validation of Cdk5-mediated KANSL1 phosphorylation in T2D mice

Further, to verify the in vitro study in vivo, we used a high-fat diet (HFD)-induced model of Type 2 diabetes (T2D) by feeding C57BL/6 mice an HFD for three months, as illustrated in Figure 7A. The development of T2D was validated by glucose tolerance test (GTT) and insulin tolerance test (ITT), which revealed that blood glucose levels were markedly increased, and insulin sensitivity was decreased in HFD-fed mice relative to those fed on a chow diet (Figure 7B–C). Western blot analysis of brain lysates showed an increase in p-KANSL1 with a decrease of PINK1 protein levels in HFD mice (Figure 7D–F). Collectively, these results reveal that Cdk5-dependent phosphorylation of KANSL1 is induced by metabolic stress associated with T2D and inversely correlates with decreased PINK1 expression in the brain. Collectively, these findings, coupled with our cellular studies, suggest a mechanism involving aberrant Cdk5 activation in the T2D brain that promotes dysregulation of the transcriptional expression of KANSL1 and ultimately contributes to impairments in mitochondrial quality control and mitophagy pathways.

Discussion

Here, the current work reveals a mechanism by which aberrant Cdk5 activation disrupts neuronal mitochondrial quality control in T2D-induced neurodegeneration. Although our previous studies identified Cdk5 hyperactivation as a major driving force underlying T2D-induced neurodegeneration [11,26,27], upstream events between Cdk5 and mitochondrial dysfunction have not been established. Here, we show that KANSL1 is a direct Cdk5 substrate and that phosphorylation

of KANSL1 inhibits PINK1-dependent mitophagy through epigenetic regulation, which offers an explanatory mechanism for the association between mitochondrial dysfunction and diabetic neurodegeneration.

Neurons are highly dependent on oxidative phosphorylation for energy production, making them particularly susceptible to defects in mitochondrial quality control. The marked reduction in basal and maximal respiration, together with diminished ATP production observed following Cdk5 activation (Figure 1), indicates that aberrant Cdk5 activity compromises mitochondrial metabolic capacity even before overt neuronal degeneration occurs. Similar bioenergetic defects have been described in the diabetic brain and are closely associated with impaired synaptic transmission and cognitive decline [28–30]. Restoration of mitochondrial respiration by TFP5 further suggests that mitochondrial dysfunction is a reversible consequence of pathological Cdk5 activation rather than irreversible metabolic damage.

Higher mitochondrial content may represent either increased mitochondrial biogenesis or reduced turnover of mitochondria. Mitophagy flux assessment in the presence of Bafilomycin A1 (Figure 2), we show that Cdk5 activation inhibits mainly mitochondrial clearance, but not biogenesis. This distinction is significant because defective mitophagy allows malfunctioning mitochondria to linger, perpetuating oxidative stress and inflammatory signaling. These observations suggest that rather than acting solely as a regulator of mitochondrial metabolism, Cdk5 acts upstream in the overall pathway controlling mitochondrial quality control.

After demonstrating that Cdk5 hyperactivity impairs mitophagy, we next sought to identify the underlying molecular target contributing to this phenotype. Interestingly, KANSL1 was identified from phosphoproteomic analysis as a potential direct substrate of Cdk5 (Figure 3). Recently, KANSL1 has been recognized as a critical regulator of mitochondrial homeostasis by transcriptionally controlling PINK1 [22,24], but its functional link to kinase-induced phosphorylation has not previously been exploited. Thus, the identification of Ser268 has enlarged the spectrum of Cdk5 substrates and uncovered a previously unappreciated link between Cdk5 signaling and chromatin regulation.

The biological significance of phosphorylation of KANSL1 cannot be determined by its identification alone. Chromatin immunoprecipitation and histone acetyltransferase assays show that KANSL1 is directly impaired by phosphorylation, evidenced by its reduced binding to the PINK1 promoter and diminished acetyltransferase activity (Figures 5E and 6F). These findings indicate that

pathological Cdk5 signaling transcriptionally represses mitochondrial quality control either through histone modifications observed in our promoter analysis or other epigenetic means, rather than by directly regulating protein activity. This type of regulation offers another level of mitophagy regulation and demonstrates how kinase signaling can modulate transcriptional programs regulating neuronal homeostasis. Importantly, increased phosphorylation of KANSL1 together with reduced PINK1 expression in HFD-fed mice (Figure 7) demonstrates that this signaling pathway is activated under T2D conditions in vivo. Previous studies from our group have already shown that Cdk5 kinase is highly dysregulated in T2D-induced cognitive impairment and that inhibition of Cdk5 can rescue its pathological conditions [11,26,27]. These findings strengthen the physiological relevance of our cellular observations and support the concept that impaired epigenetic regulation contributes to mitochondrial dysfunction during diabetes-associated neurodegeneration.

Together, our results reveal KANSL1 as a new substrate of Cdk5 and establish phosphorylation-dependent regulation coupling epigenetic dysregulation via aberrant activity of Cdk5 to impaired PINK1-dependent mitophagy. This work integrates kinase signaling with epigenetic regulation of mitochondrial quality control to provide insights into T2D-induced neurodegeneration and identify the Cdk5–KANSL1–PINK1 pathway as a target for intervention.

Acknowledgment

The authors acknowledge CSIR, SERB India, and grants GAP0168 and MLP2008 for their financial assistance and for awarding Sangita Paul and Juhi Bhardwaj senior research fellowships.

Author contributions

BK proposed the concept. SP and JB conducted the experiments. SP and BK co-wrote the manuscript. PS performed the mass spectroscopy. All authors provided constructive feedback that contributed to the study's development, analysis, and publication.

Declaration of interest

The authors declare that they have no personal or professional conflicts that could influence the research presented in this paper

References

1 Biessels GJ, Despa F. Cognitive decline and dementia in diabetes mellitus: mechanisms and clinical implications. *Nat Rev Endocrinol* 2018; **14**: 591–604.

2 Arnold SE, Arvanitakis Z, Macauley-Rambach SL, Koenig AM, Wang H-Y, Ahima RS *et al.* Brain insulin resistance in type 2 diabetes and Alzheimer disease: concepts and conundrums. *Nat Rev Neurol* 2018; **14**: 168–181.

3 De Felice FG, Ferreira ST. Inflammation, defective insulin signaling, and mitochondrial dysfunction as common molecular denominators connecting type 2 diabetes to Alzheimer disease. *Diabetes* 2014; **63**: 2262–2272.

4 Paul S, Saha D, Bk B. Mitochondrial Dysfunction and Mitophagy Closely Cooperate in Neurological Deficits Associated with Alzheimer's Disease and Type 2 Diabetes. *Mol Neurobiol* 2021; **58**: 3677–3691.

5 Crews L, Patrick C, Adame A, Rockenstein E, Masliah E. Modulation of aberrant CDK5 signaling rescues impaired neurogenesis in models of Alzheimer's disease. *Cell Death Dis* 2011; **2**: e120.

6 Dhavan R, Tsai LH. A decade of CDK5. *Nat Rev Mol Cell Biol* 2001; **2**: 749–759.

7 Pao P-C, Tsai L-H. Three decades of Cdk5. *J Biomed Sci* 2021; **28**: 79.

8 Patrick GN, Zukerberg L, Nikolic M, de la Monte S, Dikkes P, Tsai LH. Conversion of p35 to p25 deregulates Cdk5 activity and promotes neurodegeneration. *Nature* 1999; **402**: 615–622.

9 Cruz JC, Tseng H-C, Goldman JA, Shih H, Tsai L-H. Aberrant Cdk5 activation by p25 triggers pathological events leading to neurodegeneration and neurofibrillary tangles. *Neuron* 2003; **40**: 471–483.

10 Paul S, Fatihi S, Sharma S, Kutum R, Fields R, Pant HC *et al.* Cyclin-Dependent Kinase 5 Regulates cPLA2 Activity and Neuroinflammation in Parkinson's Disease. *eNeuro* 2022; **9**. doi:10.1523/ENEURO.0180-22.2022.

11 Paul S, Bhardwaj J, Binukumar BK. Cdk5-mediated oligodendrocyte myelin breakdown and neuroinflammation: Implications for the link between Type 2 Diabetes and Alzheimer's disease. *Biochim Biophys Acta Mol Basis Dis* 2024; **1870**: 166986.

12 Binukumar BK, Shukla V, Amin ND, Grant P, Bhaskar M, Skuntz S *et al.* Peptide TFP5/TP5 derived from Cdk5 activator P35 provides neuroprotection in the MPTP model of Parkinson's disease. *Mol Biol Cell* 2015; **26**: 4478–4491.

13 Binukumar BK, Pant HC. TFP5/TP5 peptide provides neuroprotection in the MPTP model of Parkinson's disease. *Neural Regen Res* 2016; **11**: 698–701.

14 Binukumar BK, Zheng Y-L, Shukla V, Amin ND, Grant P, Pant HC. TFP5, a peptide derived from p35, a Cdk5 neuronal activator, rescues cortical neurons from glucose toxicity. *J Alzheimers Dis* 2014; **39**: 899–909.

15 Shukla V, Seo J, Binukumar BK, Amin ND, Reddy P, Grant P *et al.* TFP5, a Peptide Inhibitor of Aberrant and Hyperactive Cdk5/p25, Attenuates Pathological Phenotypes and Restores Synaptic Function in CK-p25Tg Mice. *J Alzheimers Dis* 2017; **56**: 335–349.

16 Pickles S, Vigié P, Youle RJ. Mitophagy and Quality Control Mechanisms in Mitochondrial Maintenance. *Curr Biol* 2018; **28**: R170–R185.

17 Thayer JA, Petersen JD, Huang X, Gruel Budet LM, Hawrot J, Ramos DM *et al.* A unified mechanism for mitochondrial damage sensing in PINK1-Parkin-mediated mitophagy. *EMBO J* 2026; **45**: 64–105.

18 Thayer JA, Petersen JD, Huang X, Hawrot J, Ramos DM, Sekine S *et al.* Novel reporter of the PINK1-Parkin mitophagy pathway identifies its damage sensor in the import gate. bioRxiv. 2025. doi:10.1101/2025.02.19.639160.

19 Pickrell AM, Youle RJ. The roles of PINK1, parkin, and mitochondrial fidelity in Parkinson's disease. *Neuron* 2015; **85**: 257–273.

20 Fang EF, Hou Y, Palikaras K, Adriaanse BA, Kerr JS, Yang B *et al.* Mitophagy inhibits amyloid-β and tau pathology and reverses cognitive deficits in models of Alzheimer's disease. *Nat Neurosci* 2019; **22**: 401–412.

21 Narendra D, Tanaka A, Suen D-F, Youle RJ. Parkin is recruited selectively to impaired mitochondria and promotes their autophagy. *J Cell Biol* 2008; **183**: 795–803.

22 Soutar MPM, Melandri D, O'Callaghan B, Annuario E, Monaghan AE, Welsh NJ *et al.* Regulation of mitophagy by the NSL complex underlies genetic risk for Parkinson's disease at 16q11.2 and MAPT H1 loci. *Brain* 2022; **145**: 4349–4367.

23 Li T, Lu D, Yao C, Li T, Dong H, Li Z *et al.* Kansl1 haploinsufficiency impairs autophagosome-lysosome fusion and links autophagic dysfunction with Koolen-de Vries syndrome in mice. *Nat Commun* 2022; **13**: 931.

24 Hicks AR, Reynolds RH, O'Callaghan B, García-Ruiz S, Gil-Martínez AL, Botía J *et al.* The non-specific lethal complex regulates genes and pathways genetically linked to Parkinson's disease. *Brain* 2023; **146**: 4974–4987.

25 Hicks A, Reynolds R, O'Callaghan B, Ruiz SG, Martinez ALG, Botia J *et al.* The chromatin modulating NSL complex regulates genes and pathways genetically linked to Parkinson's disease. bioRxiv. 2023. doi:10.1101/2023.01.16.523926.

26 Paul S, Chandran R, Vijayan DK, Bhardwaj J, Singh P, Shetty P *et al.* A Cdk5 inhibitor restores cognitive function and alleviates type 2 diabetes in mice. *iScience* 2025; **28**: 112200.

27 Saha D, Paul S, Gaharwar U, Priya A, Neog A, Singh A *et al.* Cdk5-Mediated Brain Unfolded Protein Response Upregulation Associated with Cognitive Impairments in Type 2 Diabetes and Ameliorative Action of NAC. *ACS Chem Neurosci* 2023; **14**: 2761–2774.

28 Rolo AP, Palmeira CM. Diabetes and mitochondrial function: role of hyperglycemia and oxidative stress. *Toxicol Appl Pharmacol* 2006; **212**: 167–178.

29 Yu H, Yang C, Wang G, Wang X. Mitochondrial dynamics in diabetic peripheral neuropathy: Pathogenesis, progression, and therapeutic approaches. *Medicine (Baltimore)* 2025; **104**: e42748.

30 Baduini IR, Castro Vildosola JE, Kavehmoghaddam S, Kiliç F, Nadeem SA, Nizama JJ *et al.* Type 2 diabetes mellitus and neurodegenerative disorders: The mitochondrial connection. *Pharmacol Res* 2024; **209**: 107439.

31 Sagar S, Faizan MI, Chaudhary N, Singh V, Singh P, Gheware A *et al.* Obesity impairs cardiolipin-dependent mitophagy and therapeutic intercellular mitochondrial transfer ability of mesenchymal stem cells. *Cell Death Dis* 2023; **14**: 324.

32 Quiros PM, Goyal A, Jha P, Auwerx J. Analysis of mtDNA/nDNA Ratio in Mice. *Curr Protoc Mouse Biol* 2017; **7**: 47–54.

33 Green MR, Sambrook J. Isolation of High-Molecular-Weight DNA Using Organic Solvents. *Cold Spring Harb Protoc* 2017; **2017**: db.prot093450.

34 Utyro O, Perła-Kaján J, Jakubowski H. The Cbs Locus Affects the Expression of Senescence Markers and mtDNA Copy Number, but not Telomere Dynamics in Mice. *Int J Mol Sci* 2020; **21**. doi:10.3390/ijms21072520.

35 Nelson JD, Denisenko O, Bomsztyk K. Protocol for the fast chromatin immunoprecipitation (ChIP) method. *Nat Protoc* 2006; **1**: 179–185.

36 Vinayagamurthy S, Bhatt AK, Bagri S, Ghosh S, Parichha A, Yadav M *et al.* Non-telomeric TRF2 regulates differentiation-associated genes to maintain neural stem cell identity. *J Cell Biol* 2026; **225**. doi:10.1083/jcb.202510236.

37 Shimizu Y, Inoue A, Tomari Y, Suzuki T, Yokogawa T, Nishikawa K *et al.* Cell-free translation reconstituted with purified components. *Nat Biotechnol* 2001; **19**: 751–755.

38 Bensimon A, Heck AJR, Aebersold R. Mass spectrometry-based proteomics and network biology. *Annu Rev Biochem* 2012; **81**: 379–405.

39 Ruprecht B, Lemeer S. Proteomic analysis of phosphorylation in cancer. *Expert Rev Proteomics* 2014; **11**: 259–267.

40 Thingholm TE, Jensen ON, Larsen MR. Analytical strategies for phosphoproteomics. *Proteomics* 2009; **9**: 1451–1468.

Figure legends

Figure 1: Cdk5 hyperactivation induces mitochondrial stress and accumulation in N2A cells. (A) Schematic of the experimental design showing Cdk5/p35 or Cdk5/p25 transfection, TFP5 or scrambled peptide (SC) treatment, Seahorse mitochondrial stress analysis, MitoTracker imaging, and mtDNA copy number estimation. (B) Representative immunoblots confirming the expression of Cdk5 and Myc-tagged p35/p25 in transfected N2A cells. (C) Densitometry of Cdk5 expression after its transfection with p35 and p25. Beta-actin is used as a loading control. (D) Representative Seahorse XF24 oxygen consumption rate (OCR) profiles following sequential injections of oligomycin, FCCP, and rotenone. (E–I) Quantification of basal respiration (E), maximal respiration (F), ATP production (G), and spare respiratory capacity (H). TFP5 significantly rescued Cdk5/p25-induced mitochondrial dysfunction, whereas the scrambled peptide showed no effect. (I) Representative confocal images of MitoTracker Red-stained mitochondria (red) and DAPI-stained nuclei (blue) in NT, Cdk5/p25, and Cdk5/p25 + TFP5-treated cells. Scale bar = 2 μm. (J) Quantification of mitochondrial number per cell showing increased mitochondrial accumulation following Cdk5/p25 overexpression, which was attenuated by TFP5 treatment. (K) Relative mtDNA copy number analysis showing increased mitochondrial DNA content in Cdk5/p25-transfected cells and its restoration following TFP5 treatment. Data are presented as mean ± SEM. *P < 0.05, **P < 0.01, **P < 0.001; ns, not significant.

Figure 2: Cdk5 hyperactivity impairs PINK1-mediated mitophagy in N2A cells. Representative immunoblots and densitometric analyses showing the expression of mitophagy-related proteins in N2A cells transfected with Cdk5/p35 or Cdk5/p25 and treated with TFP5. (A–E) Cdk5/p25 overexpression reduced PINK1 expression and altered mitophagy-associated proteins, whereas TFP5 restored their expression. (F–G) Mitophagy flux was assessed in the presence and absence of Bafilomycin A1 (BafA1). Cdk5/p25 impaired mitophagy flux, while TFP5 treatment rescued mitochondrial clearance, confirming restoration of PINK1-dependent mitophagy. Data are presented

as mean ± SEM (n = 3). Statistical significance was determined by one-way ANOVA with Tukey's post hoc test. * P < 0.05, **P < 0.01, ***P < 0.001.; ns, not significant.

Figure 3: Identification of KANSL1 as a novel substrate of Cdk5/p25 by phosphoproteomic analysis. (A) Schematic of the in vitro kinase assay and LC–MS/MS workflow used to identify Cdk5/p25-mediated phosphorylation sites on KANSL1. (B) Domain structure of KANSL1 highlighting the Ser268 phosphorylation site. (C) Representative LC–MS/MS spectrum identifying phosphorylation at Ser268 (pS268). (D) Quantitative phosphoproteomic analysis showing a significant increase in KANSL1 Ser268 phosphorylation following Cdk5/p35 treatment. Data are presented as mean ± SD; * P < 0.05, **P < 0.01, ***P < 0.001.; ns, not significant.

Figure 4: Phosphorylation of KANSL1 by Cdk5 (A)Graphical representation of study design (B) Sanger sequencing data showing successful site-directed mutagenesis from TCT to GCT and TCT to GAG (C) SDS-PAGE of KANSL1 wild type, its mutants KANSL1 S>A and KANSL1 S>E expressed through in-vitro transcription and translation. (D) Graph showing Cdk5 kinase assay of both the active complexes Cdk5/p35 and 25 with KANSL1 wt and its mutants as substrates. (E)Western blot with phospho-KANSL1 and total KANSL1 antibody with the KANSL1 wt and its mutants after incubation with active Cdk5 complexes. (F) Western blot to check the expression of p-KANSL1 and total KANSL1 of wild-type and mutant plasmids in N2A cells. (G) Bar graph representing Cdk5 activity assay with KANSL1 wt and mutants expressed within the cell culture and used as substrates for Cdk5 active complexes. Data are presented as mean ± SEM; * P < 0.05, **P < 0.01, ***P < 0.001.; ns, not significant.

.

Figure 5: Cdk5-mediated phosphorylation of KANSL1 disrupts PINK1 transcription. (A) Experimental workflow for KANSL1 transfection in N2A cells. (B) Representative immunoblots showing PINK1 and KANSL1 expression following transfection with wild-type and mutant KANSL1 constructs. (C) Colocalization analysis using Immunofluorescence of KANSL1 (red), Cdk5 (green), and DAPI (blue) in N2A cells. The Pearson colocalization coefficient of KANSL1 and Cdk5 signals is calculated as 0.66. (D) Schematic of the chromatin immunoprecipitation (ChIP)-qPCR assay used to examine KANSL1 occupancy at the PINK1 promoter. (E) ChIP-qPCR

analysis demonstrating KANSL1 enrichment at the PINK1 promoter and its reduction following Cdk5/p25 expression. Data are presented as mean ± SEM (n = 3). Statistical significance was determined using one-way ANOVA with Tukey's multiple-comparison test. *P < 0.05, **P < 0.01, ***P < 0.001.; ns, not significant.

Figure 6: Cdk5-mediated phosphorylation inhibits KANSL1 histone acetyltransferase activity and suppresses PINK1 expression. (A) Experimental workflow illustrating transfection of N2A cells with KANSL1 alone or in combination with Cdk5/p35 or Cdk5/p25, followed by analysis of phospho-KANSL1 (p-KANSL1) and PINK1 expression. (B) Representative immunoblots showing p-KANSL1, total KANSL1, and PINK1 and Cdk5 protein levels. Beta-actin was used as a loading control. (C) Transfection efficiency of p35 and p25 plasmids tagged with mCherry, emitting fluorescence signals at 610 nm. (D) Relative intensity of expressions of p-KANSL1 and PINK1 protein expression. (E) Quantitative PCR analysis of PINK1 mRNA expression. (F) Histone acetyltransferase (HAT) activity assay showing the effects of Cdk5-mediated phosphorylation and KANSL1 Ser268 mutants (S>A and S>E) on NSL complex enzymatic activity. Data are presented as mean ± SEM (n = 3). Statistical significance was determined using one-way ANOVA followed by Tukey's multiple-comparison test. * P < 0.05, **P < 0.01, ***P < 0.001, ns: not significant.

Figure 7. High-fat diet-induced diabetes increases KANSL1 phosphorylation and reduces PINK1 expression in the mouse brain. (A) Experimental design illustrating the generation of the HFD-induced T2D mouse model and subsequent brain tissue analysis. (B–C) Glucose tolerance test (GTT) and insulin tolerance test (ITT) confirms impaired glucose metabolism and insulin resistance in HFD-fed mice. (D) Representative immunoblots showing phospho-KANSL1 (p-KANSL1), total KANSL1, PINK1, and Beta-actin in brain lysates from control and HFD mice. (E–F) Densitometric quantification of p-KANSL1 and PINK1 protein expression. n=6 mice per group, and all male mice were used. Data are presented as mean ± SEM. Statistical significance was determined using Student's t-test or two-way ANOVA, as appropriate. * P < 0.05, **P < 0.01, ***P < 0.001.; ns, not significant.

Tables

Table 1: List of antibodies and their dilutions used in the study

Table 2: PCR conditions used for the SDM reaction

Supplementary Files

This is a list of supplementary files associated with this preprint. Click to download.

- originaldataMtDNAcopynumber.xlsx
- TablesCelldeathanddisease.docx
- originaldataCHIPqPCR.xlsx
- originaldataPINK1RTPCR.xlsx
- originaldataCntvsHFDPINK1RTPCR.xlsx
- originaldataUncroppedblotskansl1.docx
- Figures.pdf